JOURNAL OF MATERIALS SCIENCE 32 (1997) 949–955

Cyclic fatigue of reaction-bonded silicon nitride at elevated temperatures

R. J. CHRISTENSEN*, K. T. FABER
Department of Materials Science, Robert R. McCormick School of Engineering and Applied Science, Northwestern University, Evanston, IL 60208, USA

Cyclic and static loading tests were performed on reaction-bonded silicon nitride from 1000–1400 °C in air. This porous, fine-grained material contained no glassy grain-boundary phase and exhibited no slow crack growth at room temperature. Under cyclic loading, the crack-growth behaviour at 1000 °C was similar to room-temperature results; however, at 1200 and 1400 °C crack-growth rates increased significantly. Under static loading, significant crack growth was detected at 1000 °C and increased with temperature. Most of the crack growth under cyclic loading was attributed to slow crack-growth mechanisms, but evidence of cyclic crack-growth mechanisms were also observed. Oxidation played a major role in crack-growth velocity at high temperature.

1. Introduction

The cyclic fatigue behaviour of ceramic materials at high temperatures is becoming an important design concern as ceramics are being considered for structural applications, such as heat engine components, turbine blades and tool bits. However, few cyclic fatigue tests have been performed on ceramics at elevated temperatures. Before ceramics can become viable for high-temperature applications, a greater understanding of high-temperature fatigue and the associated damage mechanisms are necessary.

Silicon nitride is one ceramic material which has received serious consideration for use in structural applications. Dense silicon nitrides are usually processed by hot pressing or sintering with additives to improve density which form a glassy phase along the grain boundaries. At elevated temperatures, this amorphous boundary phase softens, causing degradation of properties. Unlike most silicon nitride materials, reaction-bonded silicon nitride (RBSN) typically does not contain a grain-boundary phase, though it is subject to surface oxidation at temperatures above 900 °C. The aim of this study was to gain a better understanding of the cyclic fatigue behaviour at elevated temperatures of an RBSN material processed without an intergranular glassy boundary phase. The results will be compared with those found at room temperature and with other investigations, to help understand cyclic crack-growth mechanisms.

2. Background

Earlier high-temperature fatigue studies on Si_3N_4 have been restricted to those containing amorphous grain-boundary phases. For temperatures less than 1400 °C, crack growth under cyclic conditions is suppressed compared to static loading unless cyclic frequencies are low, in which case the cyclic and static rates are nearly equal. This occurs for a variety of loading conditions, including four-point bend, tension–tension, and tension–compression loading [1–6]. Under static conditions, crack growth generally occurs by slow crack-growth and creep mechanisms. The suppression of crack-growth during cycling has been attributed to transient adhesive forces in the glassy phase acting across the crack tip to shield the tip from the maximum loading stress. At lower frequencies, the transient stresses will relax, decreasing the shielding effect [2, 7]. However, a study conducted at 1450 °C on a self-reinforced hot isostatically pressed (HIPed) silicon nitride showed that the cyclic crack-growth rate exceeded the rate under static loading. The difference in behaviour was attributed to degradation of the bridging β-Si_3N_4 grains during cyclic loading [8].

A complicating factor in high-temperature fracture and fatigue of non-oxides is oxidation. At elevated temperatures under atmospheric conditions, Si_3N_4 is converted to SiO_2 at temperatures greater than 900 °C [9]. Amorphous SiO_2 first forms, then above 1200 °C, both crystalline and amorphous SiO_2 typically form [10]. The oxidation rate of RBSN is related to pore structure and temperature. Because RBSN pores are usually open, both surface and subsurface oxidation occur. As Si_3N_4 is converted to SiO_2, a volume expansion greater than 70% occurs. After some time, pores are closed off due to this large volume expansion which greatly reduces the oxidation rate. The smaller the pores, the sooner they are closed off, resulting in less extensive oxidation damage [9]. At temperatures

* *Present address*: Materials Department, University of California, Santa Barbara, CA 93106, USA.

0022–2461 © *1997 Chapman & Hall*

above 1200 °C, oxidation occurs rapidly closing off pores early, resulting in mainly surface oxidation. At temperatures below 1100 °C, more extensive subsurface oxidation occurs due to the delay of formation of this surface passivation layer [11].

Enhanced oxidation in air at regions under either tensile or compressive stress was found to occur in RBSN. Factors affecting this stress-enhanced oxidation include the amount of exposed surface area, stress, temperature, and environment [12]. These oxidation characteristics must be kept in mind while testing at elevated temperatures.

3. Experimental procedure

3.1. Material

The RBSN material (Cercom, Inc., Vista, CA) was purchased in the form of solid rods (160 mm long with a 21 mm diameter) and rectangular plates (15 mm × 54 mm × 142 mm). The material was processed with no additives or sintering aids to eliminate glassy boundary phases. The density of the material, determined by Archimedes' method, was found to be 2.17 g cm^{-3} or 68.1% theoretical density.

3.2. Flexural test conditions

Four-point bend specimens were tested on a SiC fixture with a 12.7 mm inner and 25.4 mm outer span. The fixture was loaded on a universal testing machine (MTS 808 servo-electric, MTS, Minneapolis, MN) in a modified box furnace (1706 FL(C), CM Furnaces, Inc., Bloomfield, NJ). Load was applied through self-aligning recrystallized SiC push rods (Norton Co., Worchester, MA) [13]. The furnace heating rate was 30 °C min^{-1} with a 10 min hold after reaching temperature. The specimens were loaded at a constant crosshead rate of 0.1 mm min^{-1}. Strength tests were performed at 1000, 1200 and 1400 °C, and fracture toughness tests were conducted at 920, 1200 and 1400 °C. Some room-temperature strength tests were performed on the SiC fixture which compared well with similar tests on a room-temperature fixture.

Two types of flexural specimens were used for the high-temperature fracture toughness testing. Specimens machined according to MIL-STD-1942(MR) Sample B (3 mm × 4 mm × 50 mm) were used for both strength testing and indentation strength-in-bending fracture toughness testing. Three indentation flaws made with loads of 49 or 98 N were spaced evenly along the tensile surface of the bend bar to measure fracture toughness [14]. Straight-through notched specimens were also used to measure fracture toughness [15]. These specimens had nominal cross-section dimensions of 4.9 mm × 4.9 mm and a notch-to-width ratio of 0.4.

The extent of oxidation was estimated by weighing specimens before and after high-temperature testing under both fatigue and flexural loading conditions.

3.3. High-temperature fatigue testing

Double cleavage drilled compression (DCDC) specimens with the Janssen proportions [16] were used for the cyclic fatigue and slow crack-growth testing at elevated temperatures. The specimens had a height of 42 mm, width and depth of 4.2 mm and a hole diameter of 1.12 mm. More detailed information of the geometry together with the stress-intensity calibration is discussed elsewhere [17–19].

Specimens were tested in the same furnace set-up as the flexural specimens at temperatures of 1000, 1200 and 1400 °C in air for periods of 6 h. Cyclic loading was applied at a frequency of 0.5 Hz and a stress ratio of 0.1 using a sawtooth waveform. Tests under static loading were also performed. The furnace heating rate was 20 °C min^{-1} with a hold of 15 min at temperature before specimens were loaded. *In situ* crack measurements were not possible owing to the furnace configuration which limited the amount of data obtained per specimen and precluded crack-growth measurements at higher stress intensities. Measurements were made from acetate film replicas after cooling the specimen after each 6 h test.

3.4. Electron microscopy

Post-analysis of the fatigue and flexural specimens included both scanning and transmission electron microscopy. The scanning electron microscope (JSM-6400, Joel,Tokyo, Japan) with a tungsten filament was operated at 15 kV accelerating voltage. SEM samples were coated with a thin, conductive gold layer to avoid specimen charging. The transmission electron microscope (H-700H, Hitachi, Naka, Japan) was operated at 200 kV using a tungsten filament. TEM samples were prepared by diamond-core drilling parallel to the crack front at the tip of the fatigue crack. Sections approximately 0.5 mm thick were sliced from the core-drilled sample. The slices were affixed to a glass slide and ground and polished on each side to a 1/4 μm finish and a thickness of about 100 μm. The TEM specimens were then mounted on copper grids, dimpled to a thickness of about 20 μm, and ion-beam thinned to electron transparency.

4. Results

4.1. Oxidation

Table I lists weight gains after both flexural tests (0.35 h) and fatigue tests (6.5 h). At 1000 °C very little oxidation was found to occur, even after 6 h. At 1400 °C, oxidation apparently occurred rapidly such that a protective oxide barrier was formed within minutes to protect against further oxidation. Slower, but more extensive, oxidation was found to take place at 1200 °C such that after 6.5 h twice as much weight gain was measured for a specimen at 1200 °C than at 1400 °C.

Oxidation depths were measured by a post-analysis study of specimens tested at 1200 and 1400 °C for over 6 h. By breaking these specimens at room temperature after testing, the oxidation depth into the bulk material could be observed by SEM. The oxidation depth was found to be about three times greater for the specimen tested at 1200 °C than for the specimen tested at 1400 °C, correlating well with the results in Table I.

TABLE I Oxidation weight gains during high-temperature testing

Temperature (°C)	Total weight gain (%)	
	0.35 h	6.5 h
1000	0	0.34
1200	1.5 ± 0.1	5.7 ± 0.9
1400	3.2 ± 0.5	2.8 ± 0.5

4.2. Flexural testing

The flexural strength and fracture toughness test results are plotted versus temperature in Fig. 1. The results show that the strength increases about 50% from room temperature to 1400 °C. No decrease in strength was observed up to 1400 °C, contrary to common behaviour in silicon nitrides with glassy boundary phases [20, 21]. After 0.35 h, as shown in Table I, specimens tested at 1000 °C did not show any weight gain, while significant oxidation occurred at 1200 °C. The flexural strength results show a sharp increase between 1000 and 1200 °C indicating the importance of oxidation flaw healing in strength measurements. In previous work, the strength of RBSN tested in an inert environment tended to remain unchanged from ambient temperatures up to 1375 °C [10] while experiments in air showed the strength of RBSN to increase over the same temperature range [11, 22].

The results of fracture toughness testing at elevated temperatures (Fig. 1) show a steady increase in toughness above 1000 °C. The results are both from indented and straight-through notched specimens. At 1400 °C, indented specimens did not break at the indentations because of oxidation crack healing; therefore, the toughness was determined only by the notched specimens at that temperature. Both types of specimens were used at 920 and 1200 °C, and the results from the two tests agreed well.

4.3. Cyclic and static testing

In Fig. 2, the cyclic fatigue data are plotted with static loading results by converting crack growth per cycle, da/dN, to crack velocity, da/dt, by multiplying by the frequency, ν ($da/dt = da/dN\,\nu$). Each point represents results from one 6 h test segment. The room-temperature cyclic fatigue and static loading results of RBSN [19] are included on the plot. The cyclic data at 1000 °C agreed with the room-temperature results. However, at 1200 °C crack-growth rate increased, and no fatigue threshold was detected at applied stress intensities as low as 0.55 MPa $m^{1/2}$. Under static loading, the crack-growth rate increased significantly at 1000 °C from the negligible rate measured at room temperature. At 1200 °C the static crack velocity surpasses the cyclic rate on this plot. Further, above a stress intensity of 0.6 MPa $m^{1/2}$ at 1200 °C, the statically loaded specimens were found to exhibit macrocrack deflection and branching of the primary crack which tended artificially to decrease the crack velocity.

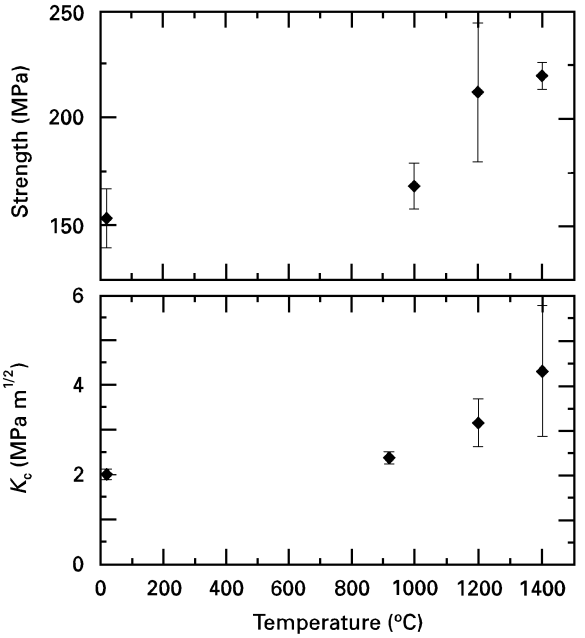

Figure 1 Flexural strength and fracture toughness values of RBSN tested in air versus temperature. The error bars indicate one standard deviation.

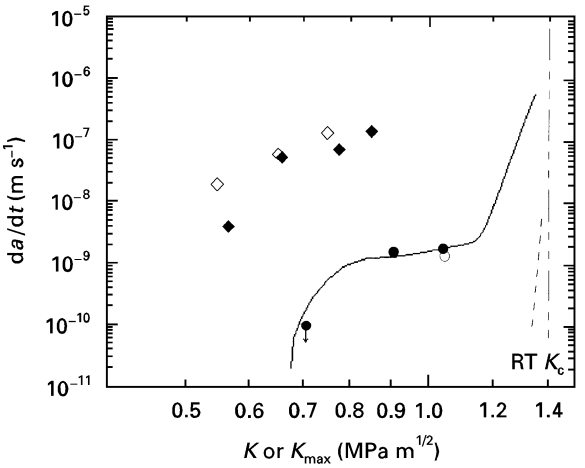

Figure 2 The crack velocity is plotted versus stress intensity for (○, ◇) static loading and (●, ◆) cyclic loading, at (○, ●) 1000 °C and (◇, ◆) 1200 °C. The data point with an arrow indicates that no crack growth was observed; room temperature results: (- - -) slow crack growth and (——) cyclic crack-growth behaviour.

Under cyclic loading at 1200 °C, the cracks were found to deflect above a maximum stress intensity of 0.7 MPa $m^{1/2}$, but crack branching was not observed; however, at 1400 °C macro-crack branching did occur, an example of which is shown in Fig. 3.

A more accurate comparison between the static and cyclic loading results can be obtained by integrating the static crack-growth velocity over one cycle of the waveform as shown by the following relation [8]

$$\frac{da}{dN} = \int_0^{1/\nu} \frac{da}{dt}\,dt \qquad (1)$$

where ν is the cyclic frequency. By assuming a simple power-law relationship for static crack growth,

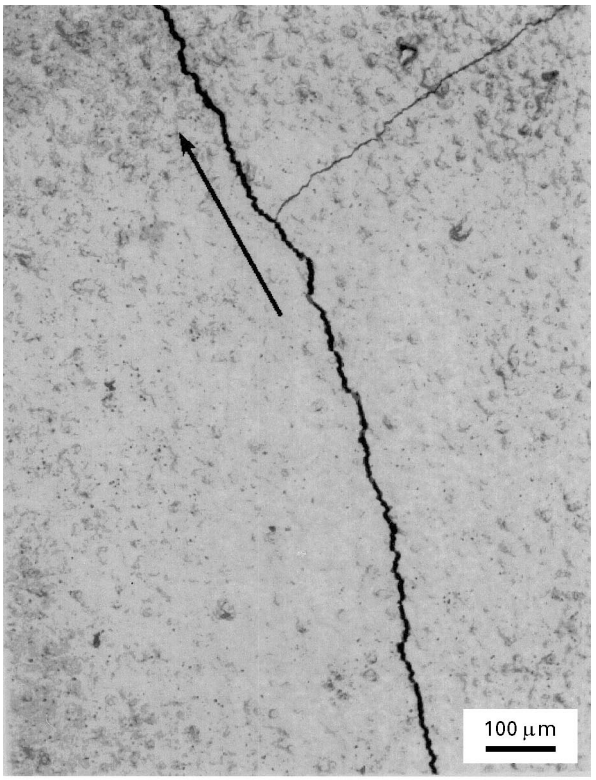

Figure 3 An optical micrograph of macro-crack branching and deflecting of the main crack in a cyclic specimen tested at 1400 °C. The crack initially grew parallel to the length of the micrograph but has slowly deflected from that direction and has branched into two cracks. The arrow indicates the direction of primary crack growth.

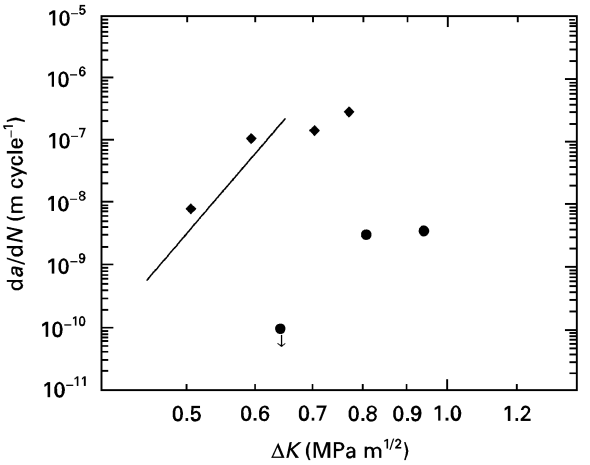

Figure 4 The crack growth per cycle plotted versus stress intensity range. The data point with an arrow indicates that no crack growth was observed. (——) Predicted cyclic crack growth from slow crack growth mechanisms at 1200 °C (Equation 2). (●) 1000 °C, (◆) 1200 °C.

TABLE II Crack growth under cyclic and static loading at 1400 °C. Note: all specimens underwent at least moderate damage

% K_c at crack tip	Static loading crack growth (mm)	Cyclic loading crack growth (mm)
70	Failure in 4 h	–
60	–	1.2[a]
50	Failure in 5 h	3.1[a]
40	–	8.0
30	1.9[a]	7.9
20	–	5.8

[a] Severe crack branching and deflecting.

$da/dt = AK^n$, Equation 1 becomes

$$\frac{da}{dN} = \int_0^{1/\nu} A[K(t)]^n dt \quad (2)$$

where K is the stress intensity factor, and A and n are material constants. Unfortunately, several of the data points collected at 1200 °C are unreliable due to the macro-crack deflection and/or branching of the primary crack, making it hard to determine an accurate curve fit for the statically loaded data. An estimate can be obtained by (a) assuming the static data have the same exponent as the cyclic data, and (b) only fitting data that did not exhibit the macro-crack damage behaviour. The result of this integration is included in Fig. 4 as the predicted crack growth at 1200 °C from the slow crack-growth behaviour. The predicted crack growth is slightly lower than the cyclic crack growth, indicating that most of the crack growth under cyclic loading at 1200 °C is due to slow crack-growth processes.

Samples tested under cyclic and static loading at 1400 °C underwent even more extensive damage exhibited as macro-crack branching and deflection. The results are contained in Table II which show crack growth at different percentages of initial critical stress intensity, K_c, of the precrack. The specimens which suffered the most severe macro-crack branching and deflection are indicated. Specimens tested under static loading either failed before the 6 h test was completed or manifested severe macro-crack branching and deflection. None of the cyclically loaded specimens failed during the test and less-severe crack branching and deflection was observed below a maximum stress intensity of 50% K_c.

Post-test analysis of the DCDC specimen revealed a residual crack opening at the crack mouth located at the edge of the hole. The openings were measured for DCDC specimens tested at elevated temperatures for the same duration and were plotted versus the initial applied stress intensity as a percentage of critical stress intensity in Fig. 5. The residual opening is an indication that permanent deformation occurred in the material. Only a small residual opening was found for samples tested at 1000 °C, but as the temperature and the applied stress intensity increased, the residual opening increased. Specimens loaded statically were found to have a larger residual crack opening than those loaded cyclically at the same temperature and duration, indicating increased permanent damage.

4.4. Electron microscopy

SEM analysis revealed micro-scale crack branching on the cyclic fatigue fracture surface of specimens tested at elevated temperatures. An example from a specimen tested at 1200 °C is shown in Fig. 6a. No obvious evidence of plastic deformation (i.e. dislocation generation) was found in TEM analysis, but microcracking and crack branching near the primary crack were common in cyclically loaded specimens.

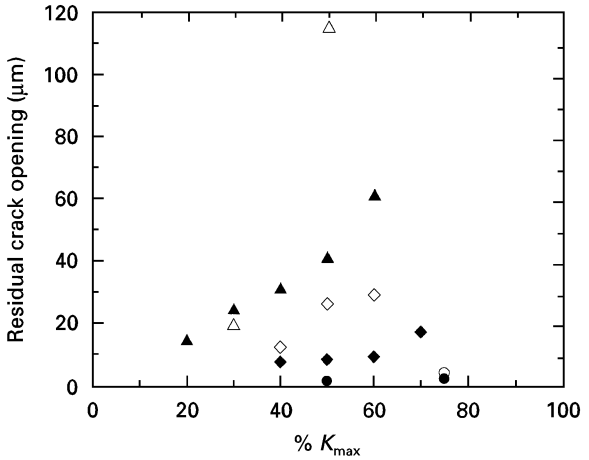

Figure 5 The residual crack opening after testing at elevated temperature versus the applied stress intensity as a percentage of critical stress intensity at (●, ○) 1000 °C (◆, ◇) 1200 °C and (▲, △) 1400 °C for (●, ◆, ▲) cyclic and (○, ◇, △) static loading.

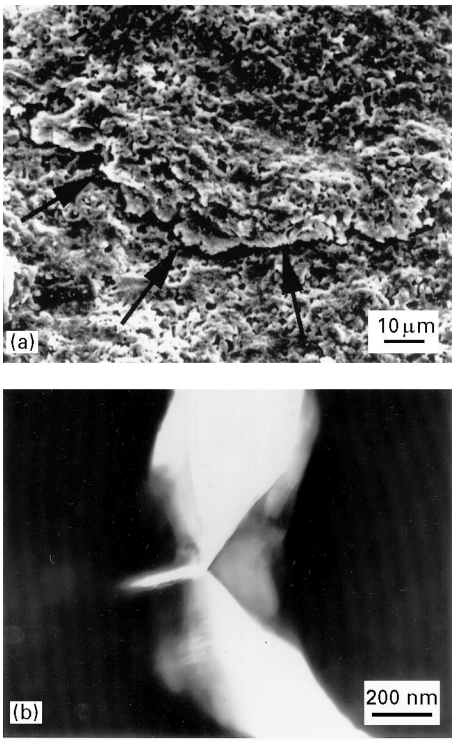

Figure 6 Examples of cyclic crack growth mechanisms. (a) Microcrack branching on the cyclic fatigue fracture surface tested at elevated temperatures. The arrows outline a lip under which the primary crack branched. (b) Secondary cracking from asperity wedging on the crack face from cyclic fatigue loading at 1200 °C. The fatigue crack runs vertically through the centre of the micrograph.

Asperity wedging also was observed via TEM of a specimen loaded cyclically as shown in Fig. 6b. These features indicate that the room-temperature cyclic fatigue mechanisms of microcracking and crack branching due to asperity wedging were active at elevated temperatures, as well.

Under static loading, rounded cavities, shown in Fig. 7, were frequently found along the edge of the primary crack. These features also were observed in specimens under cyclic loading but to a lesser extent. Rounded cavities were also observed at the tensile and

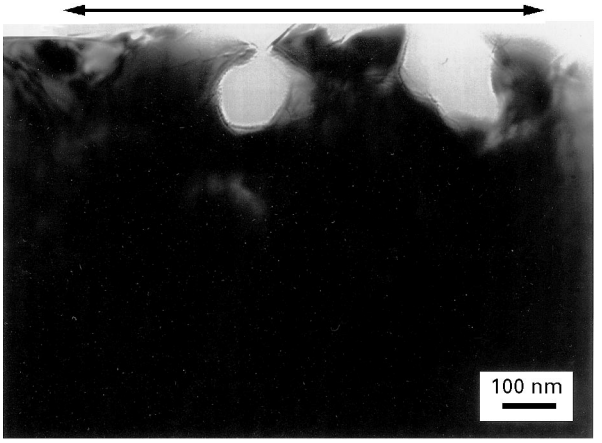

Figure 7 Rounded cavities were found along the edge of the primary crack in RBSN tested under static loading at 1400 °C. An arrow runs alongside the edge of the main crack path.

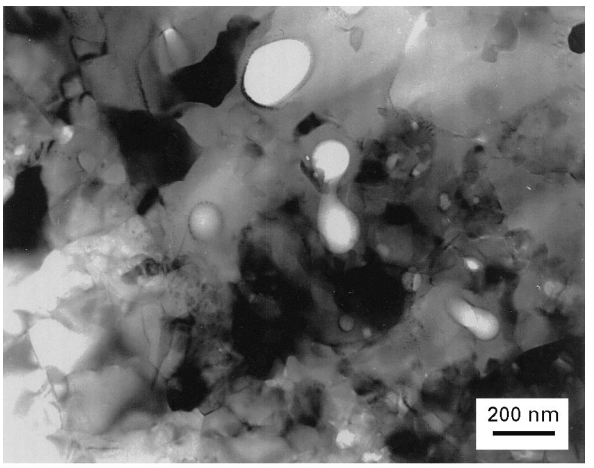

Figure 8 A transmission electron micrograph of the tensile region of a flexure specimen tested at 1400 °C.

compressive surfaces of a high-temperature flexure specimen as shown in Fig. 8, while an unstressed region located outside the loading span was found to have angular-shaped pores similar to the as-received material [19].

5. Discussion

The bending strength and fracture toughness of RBSN increase with temperature; however, increased temperature during cyclic and static loading resulted in degradation of fatigue and slow crack growth resistance. Strength and fracture toughness tests are relatively fast tests while fatigue tests are conducted over extended periods of time. The above results indicate, that over the short term, oxidation can improve mechanical properties by flaw healing. However, over longer periods of time, oxidation can be detrimental as observed in creep tests [23] and in the cyclic fatigue and static loading tests performed in this investigation.

As stated earlier, oxidation at the crack tip plays an important role in the high-temperature behaviour of RBSN. Even though RBSN does not have an intergranular glass phase at room temperature, a glass

phase (SiO_2) forms *in situ* during oxidation which is susceptible to slow crack growth in air. After the oxide layer forms at the crack tip, slow crack-growth results which exposes new silicon nitride surfaces to the atmosphere. The new surfaces oxidize and further slow crack growth occurs.

Oxidation of RBSN also makes the material susceptible to creep deformation. In an inert environment, creep of RBSN does not occur; however, in air, creep has been found to occur, although the creep rate is still considerably slower for RBSN than a typical HIPed silicon nitride [23, 24]. The circular holes observed near the primary crack in the RBSN of this study (Fig. 7) are likely sites of creep deformation. Oxidation causes amorphous and crystalline SiO_2 to form on the surface of an irregular-shaped pore near the crack tip. Cavitation acts to round pores and, in regions of high tensile stress, allows for growth of pores. Enlargement and coalescence of pores by cavitation in the high stress region near the crack tip result in creep strain and explain the residual crack openings shown in Fig. 5. The rounding of the pores is found to be stress-enhanced, because the tensile (Fig. 8) and compressive surfaces of a bend bar tested at 1400 °C contained circular pores while an unstressed region outside the loading span still contained irregular-shaped pores.

By comparing the cyclic and static results based on crack velocity (Fig. 2), it appears that specimens under static loading undergo greater crack growth at 1200 °C and above. But when the same results at 1200 °C were compared by integrating the slow crack-growth velocity over a cyclic loading cycle, the crack growth rates are nearly equal to that of cyclic loading. Most of the crack growth under cyclic loading can then be attributed to slow crack-growth mechanisms. However, the cyclic crack-growth mechanisms of crack branching and asperity wedging were also observed (Fig. 6), which may contribute a small portion to the crack growth rate at 1200 °C.

Previous studies on dense silicon nitrides indicate that cyclic loading tends to decrease crack growth at elevated temperatures, especially at high frequencies. The frequency used in this study should be high enough to achieve similar behaviour, however, crack-growth rates were nearly the same for both loading conditions. Even though RBSN forms an *in situ* oxide phase at elevated temperatures, the amount formed is significantly less than the glassy phase present in the dense sintered silicon nitride materials. Therefore, the mechanism suggested for cyclic fatigue resistance in dense silicon nitride materials, where the glassy phase shields the crack tip with transient forces, would be much less effective in RBSN. Cyclic fatigue testing of RBSN in an inert environment at elevated temperatures would certainly reveal the active mechanisms more clearly.

6. Conclusion

Flexural testing revealed increasing strength and fracture toughness with increasing temperature up to 1400 °C. The increase in strength was most likely due to flaw healing from oxidation of the material. The lack of a glassy grain-boundary phase helped maintain the strength and fracture toughness at the higher temperatures.

The DCDC specimen was successfully used for fatigue testing at elevated temperatures. Cyclic fatigue crack growth of RBSN at 1000 °C was comparable to the room-temperature behaviour; however, the crack-growth rate under static loading significantly increased at 1000 °C from ambient temperature. At 1200 °C both cyclic and static crack growth increased further. At 1400 °C, severe crack damage occurred with static loading being more detrimental than cyclic loading. Permanent deformation, manifested in residual crack opening, increased with larger applied stress intensities and increasing temperatures.

Oxidation at the crack tip was found to play an important role in the crack growth of RBSN under cyclic and static loading at elevated temperatures. Evidence includes: (a) the correlation between the large increase in oxidation rate from 1000–1200 °C and the large increase in crack-growth rates in this temperature range, and (b) at 1400 °C, the most detrimental crack growth behaviour corresponded with the fastest oxidation rate. Even though oxidation tended to improve properties of short-term tests (strength and toughness), oxidation proved to be detrimental during the longer tests of cyclic and static loading.

Comparison of crack growth under cyclic and static loading at 1200 °C by integration of slow crack velocity showed similar crack-growth rates for both loading conditions. Most of the crack growth under cyclic loading at elevated temperatures was due to slow crack mechanisms, but evidence for cyclic fatigue mechanisms also were observed under cyclic loading.

Acknowledgement

The authors gratefully acknowledge NIST for the funding support through the Program for Integrated Design, NDE, and Manufacturing Sciences.

References

1. A. G. EVANS, L. R. RUSSELL and D. W. RICHERSON, *Metall. Trans.* **6A** (1975) 707.
2. T. FETT, G. HIMSOLT and D. MUNZ, *Adv. Ceram. Mater.* **1** (1986) 179.
3. M. MASUDA, T. SOMA, M. MATSUI and I. ODA, *J. Ceram. Soc. Jpn* **97** (1989) 612.
4. T. OHJI, Y. YAMAUCHI, W. KANEMATSU and S. ITO, *ibid.* **98** (1990) 1070.
5. M. G. JENKINS, M. K. FERBER and C.-K. J. LIN, *J. Amer. Ceram. Soc.* **76** (1993) 788.
6. S.-Y. LIU, I.-W. CHEN and T.-Y. TIEN, *ibid.* **77** (1994) 137.
7. U. RAMAMURTY, A. S. KIM and S. SURESH, *ibid.* **76** (1993) 1953.
8. U. RAMAMURTY, T. HANSSON and S. SURESH, *ibid.* **77** (1994) 2985.
9. G. ZIEGLER, J. HEINRICH and G. WOTTING, *J. Mater. Sci.* **22** (1987) 3041.
10. A. G. EVANS and R. W. DAVIDGE, *ibid.* **5** (1970) 315.

11. M. E. WASHBURN and H. R. BAUMGARTNER, in "Ceramics for High Performance Applications", edited by J. J. Burke, A. E. Gorum and R. N. Katz (Brook Hill, Chestnut Hill, MA, 1975) p. 479.
12. Y. G. GOGOTSI and G. GRATHWOHL, *J. Amer. Ceram. Soc.* **76** (1993) 3093.
13. L. CHUCK, University of Dayton, personal communication (1990).
14. P. CHANTIKUL, G. R. ANSTIS, B. R. LAWN and D. B. MARSHALL, *J. Amer. Ceram. Soc.* **64** (1981) 539.
15. J. E. SRAWLEY and B. CROSS, "Cracks and Fracture", *ASTM STP 601* (American Society for Testing and Materials, Philadelphia, PA, 1976) p. 559.
16. C. JANSSEN, in "Proceedings Tenth International Congress on Glass" (Ceramic Society of Japan, Tokyo, 1974) p. 10.23.
17. H. CAI, K. T. FABER and E. R. FULLER, *J. Amer. Ceram. Soc.* **75** (1992) 3111.
18. T. A. MICHALSKE, *Engng Fract. Mech.* **45** (1993) 637.
19. R. J. CHRISTENSEN and K. T. FABER, *J. Amer. Ceram. Soc.* (1995), **79** (1996) 425.
20. S. H. KNICKERBOCKER, A. ZANGVIL and S. D. BROWN, *ibid.* **67** (1984) 365.
21. K. HATANAKA, H. SHIOTA and T. ANDO, *JSME Int. J.* **34** (1991) 351.
22. A. K. MUKHOPADHYAY and D. CHAKRABORTY, *Mater. Sci. Engng* **A122** (1989) 173.
23. G. GRATHWOHL and F. THÜMMLER, *J. Mater. Sci.* **13** (1978) 1177.
24. M. K. FERBER and M. G. JENKINS, *J. Amer. Ceram. Soc.* **75** (1992) 2453.

Received 23 February
and accepted 31 July 1996